

Note

A Novel Measurement of Voidage in Coke and Ferrous Layers in Softening and Melting under Load Test Using Synchrotron X-ray and Neutron Computed Tomography

Xinliang LIU,^{1)*} Tom HONEYANDS,¹⁾ Subhasish MITRA,¹⁾ Geoffrey EVANS,¹⁾ Belinda GODEL,²⁾ Robert George ACRES,³⁾ Floriana SALVEMINI,⁴⁾ Damien O'DEA⁵⁾ and Ben ELLIS⁶⁾

- 1) University of Newcastle, Callaghan, NSW 2308 Australia.
 2) CSIRO Mineral Resources, Kensington, WA 6151 Australia.
 3) Australian Synchrotron, ANSTO, Clayton, VIC 3168 Australia.
 4) ACNS, ANSTO, Lucas Heights, NSW 2234 Australia.
 5) BHP, Iron Ore Technical Marketing, Brisbane, QLD 4000 Australia.
 6) BHP, Iron Ore Technical Marketing, Singapore, 018983 Singapore.

(Received on April 17, 2018; accepted on July 17, 2018; J-STAGE Advance published date: September 3, 2018)

For the first time, the bed voidage of samples from interrupted softening and melting (S&M) under load tests was measured directly using computed tomography (CT). The large size, fused structure and high metallic iron content of the samples required the very high energy synchrotron X-ray source for scanning; samples produced at higher temperatures, *e.g.*, 1 450°C, required neutron CT to allow adequate penetration of the samples. This method was able to uniquely and accurately identify the volumes, distributions, and structures of coke, ferrous, and void in the S&M samples, and quantify the tortuosity of the voids. This information is critical for analysis of the pressure drop–contraction relationship in the S&M under load test, and will allow the improvement of the treatment of the cohesive zone in numerical models of the blast furnace.

KEY WORDS: voidage; void network; softening and melting; synchrotron X-ray CT; neutron CT.

1. Introduction

As a routine test, the softening and melting (S&M) under load test is used to evaluate the quality of ferrous burden materials for the ironmaking blast furnace (BF), or as a research tool to study the phenomena occurring in the cohesive zone. Useful information such as S&M temperatures, permeability, contraction and reducibility can be obtained from the test. Particularly, the measured permeability or pressure drop results are of great importance as they relate to the operational stability and productivity of the BF. To gain insights into this complex process, many studies have examined the quantitative relationship between pressure drop and bed height/contraction, using approaches such as the well-known Ergun equation,^{1,2)} Sugiyama model^{3,4)} and permeability resistance formula.^{5,6)} In those studies, the key factor bed voidage of the ferrous layer is usually assumed or estimated from physical models.

It is desirable to accurately measure the bed voidage of the samples in the S&M process, however, the relatively large

diameter (~60 mm in this work) and fused structure of the samples incorporating coke particles make it very difficult to measure using regular approaches such as mercury intrusion porosimetry. The development of the X-ray computed tomography (CT) technique has enabled researchers to study the three-dimensional (3D) microstructure of ferrous materials used in the ironmaking process, such as the porosity of sinter, granules and reduced pellet.^{7–10)} Nevertheless, to the knowledge of the authors, X-ray CT has never been used to examine the 3D structure of S&M samples. The high proportion of metallic iron (>50%) requires very high energy to penetrate the samples, *i.e.*, normal laboratory scale CT scanners are not capable of penetrating the samples.

For the first time, synchrotron X-ray and neutron CT were employed to scan the samples from interrupted S&M under load tests, uniquely reconstructing the 3D structure of the samples, identifying the coke and ferrous particles and quantifying the void fraction as a function of sample height. The methodology is presented and preliminary results are discussed.

2. Methodology

2.1. Preparation of Samples

The apparatus and detailed testing conditions for the S&M under load test have been given in a previous paper.¹¹⁾ In short, Australian porous hematite-goethite lump ore (PHGL) samples (10–12.5 mm diameter, 70 mm height) were sandwiched between two layers of coke (10–12.5 mm diameter) in a graphite crucible (60 mm inner diameter) and subjected to a programmed, time-dependent temperature profile, reducing gas flow and load. The S&M under load tests were interrupted at various temperatures by stopping the heating and changing from reducing gas to N₂. **Figure 1** shows the measured contraction and pressure drop across the burden as a function of sample temperature, with the temperatures at which tests were interrupted indicated with markers. After cooling, the graphite crucibles containing the coke and ferrous particles were set aside for CT scans.

2.2. CT Scanning

Crucibles from tests interrupted at 1 080°C, 1 200°C, and 1 300°C were scanned using X-ray CT at the Australian Synchrotron, whereas crucibles from interruptions at 1 450°C were scanned using neutron CT at the Australian Centre for Neutron Scattering (ACNS). Both beamlines are part of ANSTO's (Australian Nuclear Science and Technology Organisation) research facilities.

2.2.1. Synchrotron X-ray CT Scanning

The X-ray CT was conducted at the Australian Synchrotron's Imaging and Medical Beamline (IMBL), which uses a 4.2T superconducting multipole wiggler as its insertion device and is equipped with a double crystal-Laue monochromators.¹²⁾

For this study, hutch 3B with the sample ~135 m from the source was used with the synchrotron itself operating at 200 mA ring current and an energy of 3 GeV. Due to the highly absorbing character of the S&M samples, a filtered white beam ('pink beam'), was used instead of monochromated

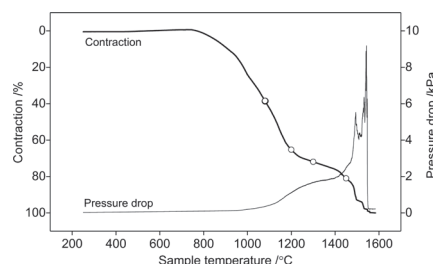


Fig. 1. Measured contraction and pressure drop results for PHGL.

* Corresponding author: E-mail: xinliang.liu@newcastle.edu.au
 DOI: <https://doi.org/10.2355/isijinternational.ISIJINT-2018-257>

X-rays because of its much higher beam flux, which improved the signal to noise ratio of the measurements. The beam was filtered by 12 mm of copper to obtain a polychromatic beam with a weighted average energy of ~150–160 keV. Projection images were collected using a pco.edge CMOS sensor fitted with an optical lens through a gadolinium oxide scintillation screen (via a 45° mirror). The effective voxel size was 31.5 μm³ and each scan consisted of 1 800 projections over 180° with an exposure time of 0.12 s per acquisition. Because of the large size of the samples, multiple scans were collected on each sample at different height levels (see Fig. 2(a)) and the individual vertical slices for each angle were combined into a single image before CT reconstruction.

2.2.2. Neutron CT Scanning

The neutron CT scan was conducted at the neutron radiography and tomography beamline called DINGO, operated by ANSTO's ACNS. The instrument, fed by the 20 MW nuclear research reactor OPAL, features a thermal neutron spectrum with a maximum intensity at 1.08 Å and full width at half maximum (FWHM) of 0.9 Å.¹³⁾

For this work, the DINGO was set up in high resolution acquisition mode and equipped with an iKon ANDOR CCD camera with 2 048 × 2 048 square pixels (16 bit). The instrument was configured with an effective voxel size of 50 μm³ over a field of view of 100×100 mm² (only one scan is needed for each sample) by coupling a 50 mm lens with a 6LiF/ZnS scintillation screen 100 μm thick. The tomographic scans consisted of 2 000 projections over 180° with an exposure time of 40 s per single acquisition.

2.3. Data Processing

2.3.1. CT Data Reconstruction

After the scanning, the vertical CT images were reconstructed and converted to a stack of two-dimensional (2D) horizontal images (see Fig. 2(b)). The synchrotron X-ray CT images reconstructions were performed using the filtered back projection method,¹⁴⁾ utilising the “X-TRACT” software package from CSIRO (Commonwealth Scientific and Industrial Research Organisation). Detector dark field noise and flat field (profile of the beam on the detector with no sample) background corrections were applied to each projection before reconstruction.

The neutron data sets were pre-processed and reconstructed by using the Octopus package.¹⁵⁾ The neutron projections were pre-processed for noise, dark field, flat field, tilt and beam-hardening corrections. The reconstruction of the 3D model was based on the filtered back projection inverse Radon transform.¹⁶⁾

2.3.2. CT Images Segmentation

After the reconstruction, each stack of 2D images (corresponding to each sample) were converted into a 3D greyscale

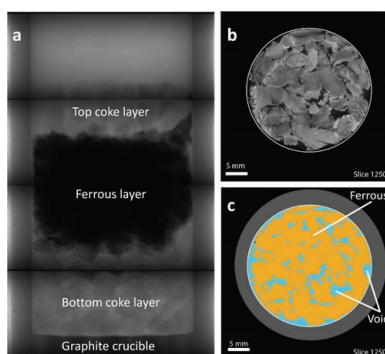


Fig. 2. Example of data processing: (a) original vertical synchrotron CT image (multiple scans); (b) reconstructed horizontal greyscale image in ferrous layer; (c) segmented and coloured horizontal image. (Online version in color.)

volume that was used for image processing and segmentation. Each 3D volume consisted of a regular volumetric grid where each voxel had a unique grey scale that was a function of the attenuation of X-rays or neutrons at that point. Prior to being segmented to delineate ferrous, coke and void, each volume was filtered using a modified version of the 3D gradient watershed segmentation algorithm described in a former work¹⁷⁾ to produce a binary image for each of the phases of interest (see Figs. 2(c) and 3). After segmentation, quantitative measurements (size and morphology) were computed on the different phases using CSIRO-developed codes to provide 3D characteristics and statistics of ferrous, coke and void (see Fig. 4).^{10,17)}

3. Results and Discussions

Figure 3 shows the reconstructed 3D structures and extracted void networks for coke and ferrous layers from the interrupted S&M under load tests. As shown, the voids, ferrous and coke particles in the S&M samples from tests

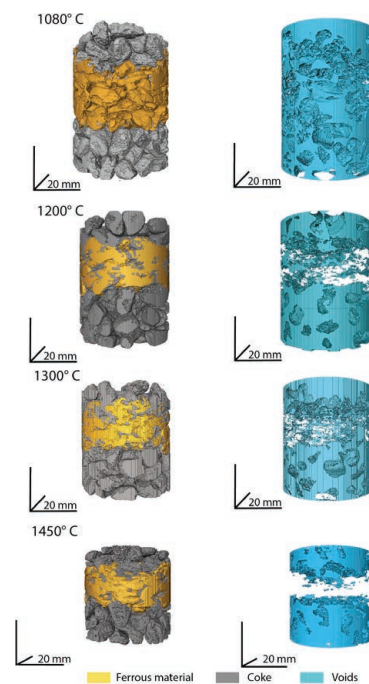


Fig. 3. 3D structure and void network of S&M under load test samples. (Online version in color.)

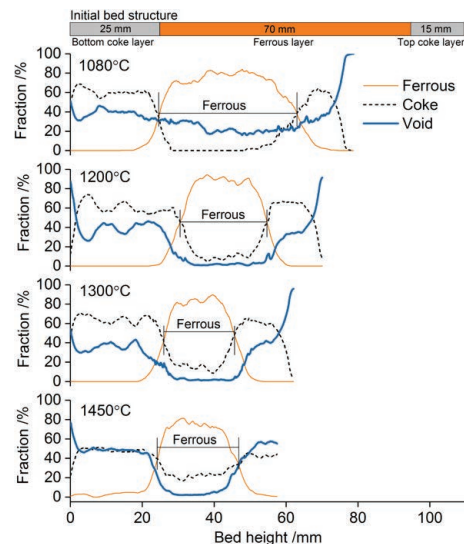


Fig. 4. Volume fraction of ferrous, coke and void as a function of bed height. (Online version in color.)

interrupted at various temperatures were all clearly identified because of their different attenuations to X-rays and neutrons. The synchrotron X-ray CT (~30 min per sample) was found to be superior to the neutron CT (>20 hr per sample) in terms of the scanning speed, but it could not effectively penetrate the metallic iron in the samples obtained above 1 300°C.

Figure 4 shows the measured volume fraction of coke, ferrous, and void as a function of bed height for each sample, with the initial bed structure indicated schematically. As observed in Fig. 3, the coke and ferrous layers became intermixed at higher temperatures. Thus, the bed heights with equal volume fraction of coke and ferrous material were chosen to delineate the boundaries between the coke and ferrous layers.

Generally, the bed voidage of the ferrous layers decreased with temperature and was always lower than that for the coke layers, and the measured vertical tortuosity of the voids varied in the range from 1.8 to 4.3. The voidage of the coke layers varied in the range 36% to 48%. This is consistent with a previous study, which showed the bed voidage in a layer of 10 mm coke particles was 41.8%.²⁾ An increase in coke voidage can be observed at the bottom and top of the crucible (0 and maximum sample height) due to the end effect.

There was a sharp decrease in the voidage of the ferrous layer from 23.2% to 2.5% when the temperature increased from 1 080°C to 1 200°C although the pressure drop across the burden didn't increase significantly (see Fig. 1). The voidage remained around 3% in the ferrous layer after the temperature reached 1 300°C. However, the voidage in the ferrous layer increased to 7% at 1 450°C, which is thought to be due to a combination of the spacer provided by coke particles present in the layer and the flow out of melt from the core of PHGL particles. As shown in Fig. 5, the optical image of the same sample for the CT scanning confirmed that large empty cores were produced at this temperature. In addition, both the optical image and the void network showed the majority of the reducing gas passed between the ferrous layer and the wall at 1 450°C.

Although coke and ferrous samples were initially loaded into the crucible in distinct layers, coke particles were identified inside the ferrous layer at higher temperatures and the volume fraction increased continuously with temperature, e.g., the coke fraction mixed in the ferrous layer was up to 24% at 1 450°C. There are three possible reasons for this: a) the rearrangement of ferrous and coke particles caused by the load,¹⁸⁾ b) the penetration of ferrous melt into the coke layers²⁾ and c) the miss-identification of coalesced slags as coke particles due to their similar attenuation coefficients or the beam hardening effect.

This quantification of bed voidage has been used to compute the pressure drop of the burden in comparison to the experimental data.¹⁹⁾ Improved pressure drop models will be developed based on this technique for inclusion in numerical models of the BF. The quantification of the 3D void structure will also allow the flow domain to be meshed for computational fluid dynamics simulation. Future work will investigate the potential to combine the optical microscopy and X-ray/neutron CT on the same sample to enhance our

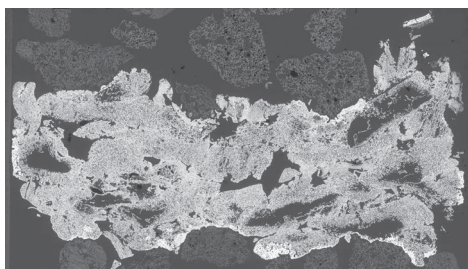


Fig. 5. Optical image of PHGL bed from interrupted S&M under load test at 1 450°C.

ability to delineate the coke/slag phase in the ferrous layer, and will consider options for the in-situ direct measurement of bed voidage in the S&M under load test.

4. Conclusions

Up until now, it has not been possible to directly measure the void fraction of samples from S&M under load test because of their size, fused structure and high metallic iron content. For the first time, a novel direct measurement approach using an X-ray beam at the Australian Synchrotron (IMBL) and a neutron beam at the ACNS (DINGO) has been applied to samples from interrupted S&M under load tests.

The CT scans were able to identify the volumes, distributions and structures of coke, ferrous, and void in the samples. The bed voidage of an Australian porous goethite-hematite lump ore decreased from ~23% to ~3% as the temperature increased from 1 080°C to 1 300°C, but increased to about 7% at 1 450°C, due in part to the influence of the intermixing of the coke and ferrous layers.

The obtained information is important to further our understanding in the S&M behaviour of ferrous burden materials. As an example, the measured voidage can be used in the calculation of the pressure drop-contraction relationship in the S&M under load test, and will allow the improvement of the treatment of the cohesive zone in numerical models of the BF.

Acknowledgements

The authors acknowledge the funding of the Australian Research Council in supporting the ARC Research Hub for Advanced Technologies for Australian Iron Ore and BHP for their financial support and permission to publish this paper. The authors are grateful to Australian Synchrotron and ACNS for scanning the samples, and Mr. Gareth Penny for his assistance with the experimental work.

REFERENCES

- 1) S. Ergun: *Chem. Eng. Prog.*, **48** (1952), 89.
- 2) K. Ichikawa, Y. Kashihara, N. Oyama, T. Hirose, J. Ishii, M. Sato and H. Matsuno: *ISIJ Int.*, **57** (2017), 254.
- 3) K. Ichikawa, J. Ishii, S. Watakabe and M. Sato: *ISIJ Int.*, **55** (2015), 544.
- 4) J. Ishii, R. Murai, I. Sumi, Y. Yongxiang and R. Boom: *ISIJ Int.*, **57** (2017), 1531.
- 5) K. Takatani and Y. Iwanaga: *Tetsu-to-Hagané*, **73** (1987), 980.
- 6) K. Kodama, T. Horio and Y. Hida: *Tetsu-to-Hagané*, **52** (1966), 295.
- 7) V. Shatokha, I. Korobeynikov, E. Maire, L. Grémillard and J. Adrien: *Ironmaking Steelmaking*, **37** (2010), 313.
- 8) V. Shatokha, I. Korobeynikov, E. Maire and J. Adrien: *Ironmaking Steelmaking*, **36** (2009), 416.
- 9) E. Hjortsberg, F. Forsberg, G. Gustafsson and E. Rutqvist: *Ironmaking Steelmaking*, **40** (2013), 399.
- 10) B. Godel, B. Ellis, D. O'Dea, T. Honeyands and T. Harvey: *Iron Ore 2017*, The Australasian Institute of Mining and Metallurgy Melbourne, (2017), 529.
- 11) C. E. Loo, L. Matthews and D. O'Dea: *ISIJ Int.*, **51** (2011), 930.
- 12) A. W. Stevenson, J. C. Crosbie, C. J. Hall, D. Hausermann, J. Livingstone and J. E. Lye: *J. Synchrotron Radiat.*, **24** (2017), 110.
- 13) U. Garbe, T. Randall, C. Hughes, G. Davidson, S. Pangelis and S. J. Kennedy: *Phys. Procedia*, **69** (2015), 27.
- 14) T. Gureyev, Y. Nesterets, D. Ternovski, D. Thompson, S. Wilkins, A. Stevenson, A. Sakellariou and J. Taylor: *Advances in Computational Methods for X-Ray Optics II*, Society of Photo-optical Instrumentation Engineers (U.S.), Bellingham, (2011), 81410B.
- 15) M. Dierick, B. Masschaele and L. Van Hoorebeke: *Meas. Sci. Technol.*, **15** (2004), 1366.
- 16) H. Barrett and W. Swindell: *Radiological Imaging: The Theory of Image Formation, Detection and Processing*, Academic Press, New York, (1981), 536.
- 17) B. Godel: *Econ. Geol.*, **108** (2013), 2005.
- 18) C. E. Loo, G. Penny, L. Matthews and B. Ellis: *Proc. 10th CSM Steel Cong. and 6th Baosteel Biennial Academic Conf.*, Metallurgical Industry Press, Beijing, (2015), 1.
- 19) S. Mitra, X. Liu, T. Honeyands, G. Evans and D. O'Dea: *Proc. 3rd Int. Conf. on Science and Technology of Ironmaking and Steelmaking (STIS)*, Solar Press, Kanpur, (2017), 207.